DOI: 10.1002/cctc.200((will be filled in by the editorial staff))

Viability of Au/CeO_2-ZnO/Al_2O_3 catalysts for pure hydrogen production via WGS

Tomás Ramírez Reina[*a], Svetlana Ivanova[a], Juan José Delgado[c], Ivan Ivanov[b], Vasko Idakiev[b] ,Tatyana Tabakova[b], Miguel Angel Centeno[a], José Antonio Odriozola[a]

The production of H_2 pure enough to use it in fuel cells requires the development of very efficient catalysts for the WGS reaction. In this study a series of gold catalysts supported on ZnO-promoted CeO_2-Al_2O_3 is presented as interesting systems for the purification of H_2 streams via WGS. The addition of ZnO remarkably promotes the activity of a $Au/CeO_2/Al_2O_3$ catalyst. This increase in activity is mainly associated to the enhanced OSC exhibited for the Zn-containing solids.
Not only high activity but also good stability and resistance towards start-up/shut-down situations was found making these catalysts a promising alternative for CO-clean up applications.

Introduction

The experience gained from over a decade of sustained research, development and demonstration projects confirms that hydrogen and fuel cell (FC) technologies have a strong potential to play a decisive role in the new energy system for the coming years [1]. Hydrogen is an energy carrier that has to be produced from hydrogen containing molecules such as hydrocarbons, ammonia or chemical hydrides [2]. The best short-term option seems to be the production of hydrogen through the hydrocarbon reforming. However the reformate is a mixture of hydrogen and carbon oxides as main products [3]. The presence of insignificants amounts of CO in hydrogen flows inactivates fuel cell electrodes. To avoid the poisoning of the fuel cell anode, several fuel processing steps, including CO removal by means of the water gas shift (WGS) and CO preferential oxidation reactions (PrOx) must be applied. The development of efficient catalysts for these processes is fundamental for the success of the so called "hydrogen economy".

Among the studied catalysts, gold-based materials have been broadly employed for the WGS obtaining hopeful results in many cases [4]. The high activity of gold catalysts for this process is commonly associated to the gold particles size, dispersion and interaction with the support. All of these aspects can be controlled by the preparation method [5]. The advantages of gold based catalysts for the WGS have been recently summarized by Burch [6]. In this work the debate about the reaction mechanism is addressed. Conventionally, two main mechanism are proposed for the WGS; i) the so-called redox mechanism (or surface mechanism), where CO adsorbs on gold particles and reacts with oxygen from the support, which, in turn, is reoxidised by water and, ii) the associative mechanism, also called formate mechanism, where formate species are generated from the interaction of CO with OH from the support. The decomposition of these intermediates yields to the reaction products, CO_2 and H_2. In addition Burch proposed an universal mechanism for the WGS which is consistent with much of the experimental data from the literature.

As a very relevant remark, it should be mentioned that the reaction conditions (CO and H_2O concentrations, presence or not of CO_2 and H_2 in the feed, etc.) modulate the predominant mechanism. In addition, as the WGS is a reversible reaction, a strong inhibition of the catalyst performance is found when the reaction products (CO_2 and H_2) are included in the stream.

On the other hand, the choice of the support is particularly of relevance in order to obtain high performances in this kind of CO elimination reaction. Ceria has became one of the most popular and successfully employed support for gold nanoparticles in the low temperature WGS and in the PrOx reaction during the last decade [4e, 7]. The suitability of cerium oxide for oxidation catalysis is related to its redox behavior (Ce^{4+}/Ce^{3+}) and oxygen storage/release capacity resulting from the oxygen mobility in its lattice [8]. Under moderate temperatures and reductive conditions, such as WGS atmosphere, oxygen vacancies can be created in CeO_2 leading to the formation of non stoichiometric oxides CeO_{2-x} ($0< x < 0.5$) [9]. The concentration of these structural defects has been correlated with the catalytic activity in CO elimination reactions [10]. Recently, the use of ZnO has been proposed as an efficient structural defect promoter of cerium oxide [4e]. The epitaxial interaction between both oxides may create preferential sites for gold deposition in the oxides interphase leading to a high gold dispersion and improved catalytic activity. Laguna and coworkers reported that Zn-modified gold catalysts are more active than the un-promoted Au-CeO_2 system in the direct CO oxidation reaction [11]. A point to consider is that the WGS reaction involves the participation of the available oxygen of the support when the redox mechanism is dominant. In this sense, efficient catalysts for this process should present high oxygen mobility facilitating the oxygen transfer reactions. The participation of oxygen atoms not only from the surface but also from the bulk

together with an enhanced reducibility constitutes an important skill for an efficient WGS catalyst. Dispersing ceria over a high surface carrier such as alumina opens up the possibility of having higher surface/bulk ratio thus likely improving the oxygen mobility. The use of ZnO as a ceria promoter may contribute to achieve the mentioned properties.

In this context, the aim of the work is to study the viability of the ZnO-promoted $Au/CeO_2/Al_2O_3$ catalysts the WGS reaction towards H_2 clean-up reactions.The correlation of the catalytic behavior with the physicochemical properties, as for example the oxygen storage capacity and the UV-vis features is also a subject of this study and it will be used to justify the suitability of the presented systems for the CO-free hydrogen production.

Results and Discussion

Results and discussion

Chemical composition and textural properties

Chemical composition and textural properties of the prepared catalysts are presented in **Table 1**. All the systems contain cerium oxide loadings close to the nominal value (15 wt.%). The final amount of zinc oxide in the ceria-doped supports resulted to be approximately 50 % of the intended value. The loss of ZnO could be related to the ammonia treatment employed during the synthesis in order to assure the complete conversion of the nitrates.

Gold deposition did not cause any remarkable change in the catalysts composition. The amount of cerium and zinc oxides remains close to the one obtained for their corresponding support.

In all catalysts, the gold content is very close to 2 wt%, which confirms that the gold deposition was performed successfully, except for the Au/Al and Au/Zn/Al catalysts for which the gold content is quite lower than the target one. The smaller gold uptake exhibited for the alumina support agrees with previous results obtained by Ivanova and collaborators using the same gold deposition method [12].

Concerning the textural properties, all the samples are mesoporous materials with pore sizes around 70 Å with specific surface area neighboring that of the primary support (γ-Al_2O_3). No matter the doping metal oxide or the gold presence, the specific surface area seems to be governed by the primary support. In addition the presence of gold increases the surface area in all the samples respect to their corresponding supports (**Table 1**). The increase of the surface area is related to the observed increase of the pore volume. This effect agrees with the results previously observed and explicated by Somorjai et al. [13] claiming that the inclusion of gold nanoparticles in the pore structure would lead to a pore widening and therefore an increase on the specific surface area.

XRD:

XRD patterns of the prepared supports are shown in **Figure 1A.** For every sample the XRD pattern shows diffraction lines

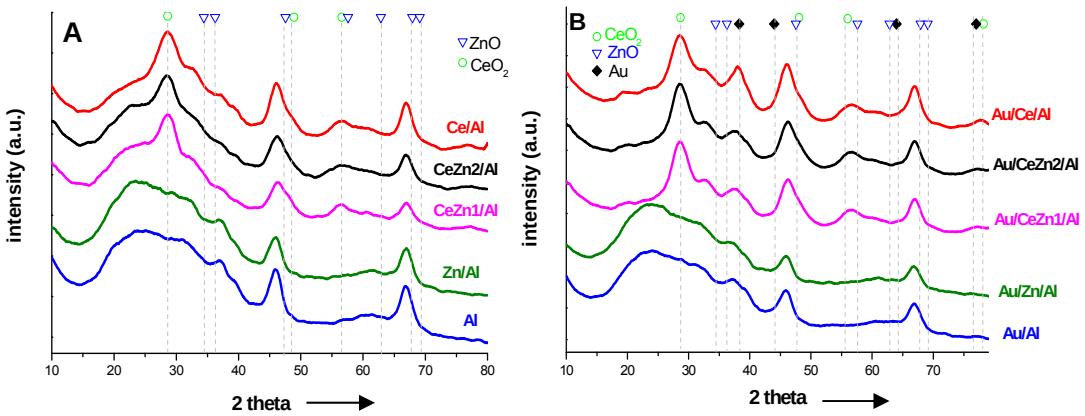

Figure 1: XRD patterns of the prepared materials: A) supports; B) gold catalysts

Table 1. Chemical composition and main textural properties of the prepared solids

Sample[a]	CeO_2 (wt.%)	ZnO (wt.%)	Al_2O_3 (wt.%)	Au (wt.%)	S_{BET} (m^2/g)	Average pore size (Å)	Pore volume (cm^3/g)
Al	-	-	100		202	74	0.5126
Ce/Al	14.62 (15)	-	85.38 (85)	-	186	69	0.4176
Zn/Al	-	2.96 (15)	97.04 (85)	-	184	72	0.4867
CeZn1/Al	15.78 (15)	0.47 (1)	83.75 (84)	-	179	64	0.3958
CeZn2/Al	14.40 (15)	1.2 (2)	84.40 (83)		185	68	0.4367
Au/Al	-	-	98.84 (98)	1.16 (2)	217	75	0.5608
Au/Ce/Al	14.70 (15)	-	83.62 (83)	1.68 (2)	197	69	0.4545
Au/Zn/Al	-	2.53 (13)	96.79 (85)	0.69 (2)	213	74	0.5580
Au/CeZn1/Al	13.84 (15)	0.40 (1)	83.89 (82)	1.87 (2)	192	65	0.4171
Au/CeZn2/Al	13.37 (15)	1.05 (2)	83.59 (81)	1.99 (2)	181	68	0.4064

[a]: nominal values in parenthesis.

corresponding to the cubic CeO_2 fluorite type structure (JCPDS# 00-004-0593) and to the γ-Al_2O_3 phase (JCPDS# 00-048-0367). No signals due to the crystalline ZnO were found. The slight quantity of doping oxide, a rather high dispersion, or the amorphous character of the ZnO may account for this fact. The calculation of the ceria partcile size by Scherrer ecuation revealed that the introduction of gold and cinc did not substancially modifies the size of cerium oxide particles which is always around 5 nm.

The diffraction patterns of the prepared gold catalysts are shown in **Figure 1B**. All the systems manifest similar XRD

[a] *Tomás Ramírez Reina*, Svetlana Ivanova, , Alejandro Pérez Flórez, Miguel Angel Centeno and José Antonio Odriozola.*
Departamento de Química Inorgánica e Instituto de Ciencia de Materiales de Sevilla, Centro mixto Universidad de Sevilla-CSIC, Avda. Américo Vespucio 49, 41092 Sevilla, Spain
[b] *Ivan Ivanov, Vasko Idakiev and Tatyana Tabakova*
Institute of Catalysis, Bulgarian Academy of Sciences, Acad. G. Bonchev str., bl. 11, Sofia, 1113 Bulgaria
[c] *Juan José Delagado Departamento de Ciencia de los Materiales e Ingeniería Metalúrgica y Química Inorgánica, University of Cádiz, Apdo. 40 Puerto Real, Cádiz 11510, Spain*

**E-mail: tomas.ramirez@icmse.csic.es*

diagrams corresponding to the primary support. No signals due to metallic gold could be detected indicating that gold particles are small (or at least they are beyond the detection limit of the equipment, 4 nm) and well dispersed on the support.

TEM

Selected TEM images of the supports and gold catalysts are shown in **Figure 2A** and **2B** respectively. The white spots correspond to the presence of heavier elements such as Ce, Zn and/or Au supported on alumina. In the case of the supports, cerium oxide and cinc oxide are homogeneously deposited and well dispersed on the primary alumina support. It is not possible to distinguish among cinc oxide and ceria in the TEM micrograps because of the lack of contrast. In general, ceria particle size is close to 5 nm in good agreement with the XRD data. However some polycrystalline ceria agglomerations were detected presenting higher size.

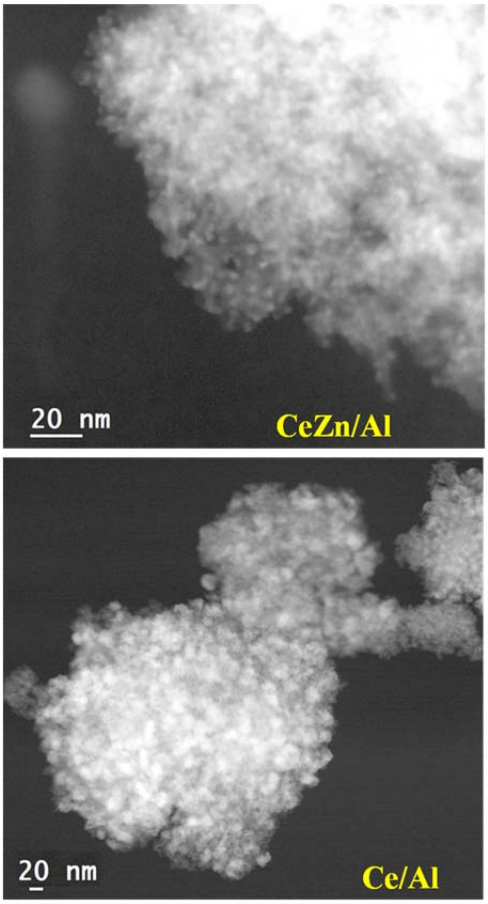

Figure 2A: Selected TEM images of the supports

Regarding the gold catalysts (**Figure 2B**) no clear differences in dispersion, size and shape are evidenced among the samples. The high atomic weight of cerium atoms in the samples makes the detection of gold particles difficult due to the low mass and diffraction contrast. However gold nanoparticles are highlighted as the most brilliant spots in the picture in comparison to the supports images. Even in this situation it is difficult to evaluate the gold particle size. Mainly, all the particles studied are agglomerations of gold and ceria and/or gold-ceria-cinc oxide with particle sizes ranging from 3 to 5 nm. Unfortunately it is not possible to measure only gold within the agglomerates but it is obvious that average gold particle size must be smaller than the agglomerate one (less than 5 nm) in good agreement with the XRD data. The later, makes us to consider 4 nm as average gold particle size for further calculations in the paper.

In addition, EDX spectra (see supporting information) revealed that gold is mainly associated to ceria and not to the primary alumina support. This preferential nucleation of gold over cerium oxide was previously observed by Centeno and collaborators denoting a strong Au-Ce interaction [14]. For the doped sample, ZnO particles were also detected in intimated contact with the Au-CeO_2 clusters. From here it can be concluded that Au-CeO_2-ZnO interactions must be expected for this catalysts leading to a metallic synergistic effect that can influence the performance of the materials.

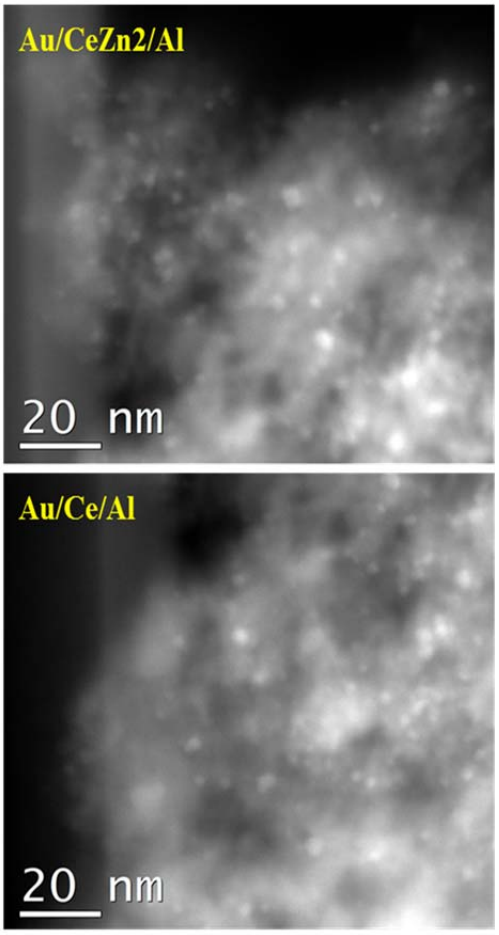

Figure 2B: Selected TEM images of the gold catalysts

UV-Vis

UV-vis spectra of the prepared supports are presented in **Figure 3A**. Quite relevant information regarding the nature of the samples can be extracted from the spectra interpretation. First, related to the doping agent, ZnO, which was not possible to detect by XRD, appears in the UV-vis experiment. ZnO is a wideband-gap semiconductor (Eg = 3.37 eV) with a large excitation binding energy (60 meV) [15] . The absorption peaked at 340 nm in the Zn/Al sample could be attributed to a well-defined excitation band of ZnO in agreement with the absorption band observed for ZnO nanorods in ref. [14]. The estimation of the ZnO direct band gap by plotting $[(F(R)hv]^{1/2}$ against energy and the linear part of the curve extrapolated to $[(F(R)hv]^{1/2} = 0$ results in a value of 3.12 eV very close to that obtained by Ahmed et. al [16].

The band structure of the ZnO suggests that there are two types of electronic transitions: the transitions between the filled O 2p orbitals and the empty Zn 4s orbitals with the possibility of some Zn 4p orbitals [16]. Furthermore, the average ZnO particle size can be calculated from the UV-Vis absorption spectra using a mathematical model proposed in ref. [17]. In this model they establish the relation between the maximum of the absorption edge and the particle size. In our case ZnO nanoparticles present an average particle size of 1.86 nm thus explaining the absence of XRD peaks related to any ZnO phase. In addition, the broad band situated at about 350 nm in the UV region accounts for the ceria UV-vis features. This band is due to the charge transfer from 2p valence band of O^{2-} to 4f band of Ce^{4+} [18]. For the ternary Ce-Zn-Al systems widening and shifting of the absorption edge is observed evidencing Ce-Zn interaction in good agreement with the microscopy results.

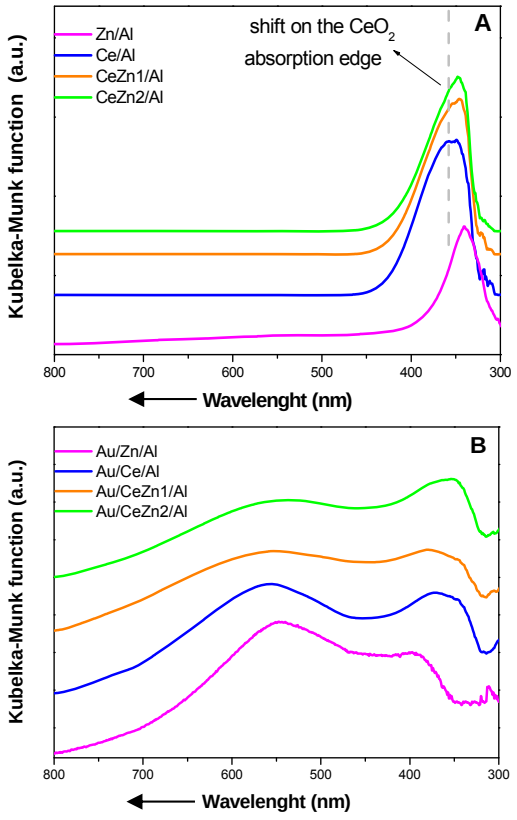

Figure 3: UV-Vis spectra of the studied systems: A) supports; B) gold catalysts

For further understanding about this fact, ceria band gap of the prepared supports was estimated and the results are summarised in **Table 2**. The direct band gap for the Ce/Al solid is very close to the one reported in the literature for a similar system [18]. A slight increase of the band gap is observed for the Zn-promoted samples evidencing the modification of the ceria electronic properties due to the presence of ZnO. The occupation of the ceria valence band is lower when ZnO is present. In other words, ZnO promotes an electronic deficiency on the ceria band structure. Laguna and coworkers proposed a mechanism that can be helpful to explain this fact [10]: The reaction of lattice oxygen of ZnO, O_o^x, with cerium oxide (III) may lead to the oxidation of cerium with the formation of oxygen vacancies, V_o^x , on ZnO lattice when ceria and zinc oxides are in close contact as follow:

$$Ce_2O_3 + O_o^x \leftrightarrow 2CeO_2 + V_o^x$$

According to the thermodynamic shown in [19], the free energy for this process is given by $\Delta G = -54.310 + 8T$ (J/mol) where ΔG is the free Gibbs energy and T is the temperature. Therefore the formation of oxygen vacancies on the ZnO lattice accounts for the lower occupation of the ceria valence band. The increase of the Ce^{4+} species involves a decrease of the cerium oxide particle size thus changing the surface-to-volume ratio. The change of the surface-to-volume ratio also affects the ceria reducibility as explained in ref. [11] and contribute to the band gap modification.

Table 2. Ceria band gap energies for the prepared materials

Sample	Direct band gap (eV)	Indirect band gap (eV)
Ce/Al	3.04	2.82
CeZn1/Al	3.09	2.92
CeZn2/Al	3.11	2.95
Au/Ce/Al	2.37	1.77
Au/CeZn1/Al	1.92	1.32
Au/CeZn2/Al	2.41	1.81

The diffuse reflectance spectra of the prepared gold catalysts are presented in **Figure 3B.** For all the samples a broad absorption band was found in the range 500-570 nm. This contribution is assigned to the plasmon resonance of gold nanoparticles. ZnO absorption edge was shifted towards higher wavelengths due to the Au-Zn contact confirming a modification of ZnO band structure when gold is present. In addition, a shift on the ceria absorption edge provoked for the gold deposition was also observed. It should be noted that this shift is quite more marked than the one caused for the addition of the promoters (Zn) to the bare Ce/Al support. The later denotes that the Au-Ce interaction is stronger and more relevant than the Ce-Zn interaction in terms of modification of the ceria electronic properties. Furthermore, despite the difficulty of the estimation because of the presence of the gold plasmon (especifically in the Au/CeZn1/Al sample), a contraction of the ceria band gap is detected for the gold samples **(Table 2)**. For all the catalysts, both direct and indirect band gaps are smaller than that of the parent support. The later evidences a strong electronic metal-support interaction. The decrease in the ceria band gap could indicate the presence of partially reduced ceria on the surface of the catalysts, in good agreement with the results of Acerbi and collaborators [20]. This "electronic metal-support interaction" (EMSI) influences on the ability of the catalysts to bond to a number of adsorbates thus modulating the catalytic activity.

OSCC, OSC and reducibility

Deeper insights of the promoting effect of ZnO addition to the ceria redox properties was obtained by the calculation of the oxygen storage complete capacity (OSCC) and the oxygen storage capacity (OSC) of Ce/Al and CeZn2/Al samples and their corresponding gold analogues. The OSCC provides information about the maximum reducibility of the samples while the OSC informs about the most reactive and most available oxygen atoms.

The OSCC and OSC are expressed in μmol $CO_{2\ /g\ sample}$ from the CO consumption or CO_2 formation (after CO pulses). The OSCC results at different temperatures are presented in **Figure 4**. As a general trend, the increase of the temperature increases the OSCC value. For all the studied temperatures the Zn containing materials exhibited higher OSCC compared to the un-modified ones. This result indicates that the inclusion of ZnO in the catalyst formula promotes the oxygen mobility. In addition, the gold catalysts presented much higher OSCC than their parent supports indicating the great increase of the oxygen mobility in the ceria lattice when gold is present. The result agrees with that obtained by Bedrane and collaborators [21]. The oxygen storage capacity is widely enhanced by the presence of metal particles in the surface. They claimed that metal particles may act as portholes for the subsequent migration and storage of oxygen on the support [21].

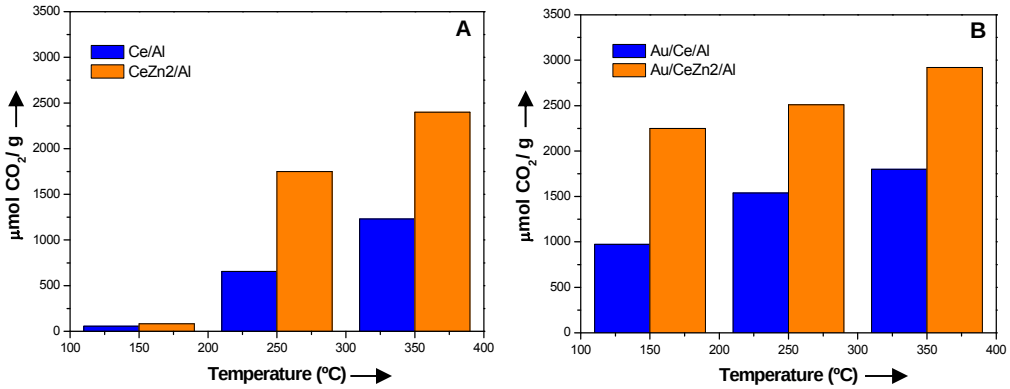

Figure 4: OSCC of the prepared materials: A) supports; B) gold catalysts

In order to find out the number of oxygen layers involved in the process, measurements of the OSC were carried out. For the OSC theoretical calculations, the number of surface oxygen atoms and the BET area of each sample (**Table 3**) were considered. The calculations have been made following the methodology proposed by Duprez et. al [22]. More precisely it was considered that i) only oxygen atoms bonded to the cerium ones participate in the oxygen storage process; ii) the surface is considered homogeneous iii) only one of the four oxygen atoms is involved in the storage ($CeO_2 \rightarrow Ce_2O_3$ + "O"); and iv) null gold metal contribution to the reduction, e.g. the gold metal could not be reoxidized after the calcinations of the samples. In a similar way, as observed in the OSCC, the OSC of the Zn-modified samples is higher than the corresponding un-promoted ceria ones. Almost no oxygen mobility was detected for the supports at the lowest examined temperature (150ºC). Nevertheless, a remarkable effect of gold in the reducibility of ceria is observed. The presence of gold leads to the increase of OSC in the whole temperature range. It should be noticed that this effect is less notorious at 350ºC indicating that ceria is partially reduced and the reduction process influences the oxygen mobility.

The number of atomic oxygen layers (NL) that participates in the redox process has been also estimated and the results are summarized in **Table 3**. The higher the temperature, the higher the NL for all the studied cases. At the lowest temperature (150ºC) almost no oxygen mobility was observed for the supports. However the presence of gold induces an increase of the NL value of about 20 and 40-fold for the Ce/Al and for the CeZn2/Al respectively. At 250ºC and 350ºC all the solids presented NL higher than one indicating the participation of bulk oxygen atoms. This effect is particularly notable for the Ce-Zn mixed system where the oxygen mobility is always superior compared to that of the un-promoted ceria systems, except at 150ºC where poor oxygen mobility was found in both samples. It is worth to note that for the Au/Ce/Al sample not appreciable increase of the NL was detected between 250ºC and 350ºC pointing that a maximum of oxygen mobility is reached. This restriction was not found for the Au/CeZn2/Al that displayed very high oxygen mobility at 350ºC with the participation of eight layers of bulk oxygen. The results obtained here are comparable to that presented in ref [22] for a CeO_2 and CeO_2-ZrO_2 systems promoted with Pt, Rh and Ru. Furthermore, the enhanced reducibility and oxygen mobility of the gold catalysts agrees with the above commented UV-vis data in terms of electronic metal-support interaction. In a similar way than in ref [20], a promoted reducibilty of ceria and a rearrangement of the ceria band structure are observed due to the precious metal-support interaction.

The stoichiometry of the "reduced" cerium oxide (CeO_m) can be calculated by the following equation:

$$m = 2 - (M \times OSCC \times 10^{-6}) \quad (1)$$

Furthermore the reducibility of ceria has been estimated using equation (2)

$$\text{Red. } (\%) = (2-m/2-x) \times 100 \quad (2)$$

Being *x* the stoichiometry obtained for the maximum ceria reduction, when all the Ce^{4+} ions are transformed to Ce^{3+} leading to $CeO_{1.5}$. The results of these calculations are presented in **Table 4**. For both supports, the *m* parameter decreases whit the temperature increase indicating a high degree of ceria reduction. Indeed the reducibility data clarify that ceria reduction increases with the temperature. At the lowest temperature tested almost no reduction of ceria was found for both systems. In good agreement with the OSC studies, the Zn-promoted sample presented higher reducibility that the bare Ce/Al solid in the whole temperature range confirming the promotion of the ceria redox properties by the presence of ZnO. Complete reduction of ceria was found at 350ºC for the CeZn2/Al support.

Table 3. Oxygen storage capacity (OSC) and number of oxygen layers (NL) as a function of the temperature

Sample	$OSC_{150ºC}$	$OSC_{250ºC}$	$OSC_{350ºC}$	$NL_{150ºC}$	$NL_{250ºC}$	$NL_{350ºC}$
Ce/Al	15	209	479	0.10	1.36	3.11
CeZn/Al	13	403	778	0.08	2.72	5.26
Au/Ce/Al	370	651	672	2.11	4.11	4.24
Au/CeZn2/Al	594	743	950	4.13	5.20	8.03

Table 4. Stoichiometry (m) and reducibility (% Red) of ceria in the prepared supports

Sample	Temperature (ºC)	m in CeO_m	% Red
Ce/Al	150	1.99	1.92
Ce/Al	250	1.89	22.56
Ce/Al	350	1.79	42.3
CeZn2/Al	150	1.99	2.81
CeZn2/Al	250	1.70	60.2
CeZn2/Al	350	1.46	100

Dispersing cerium oxide on alumina and adding ZnO as a promoter results in complete and fast availability of oxygen for the reaction.

Water Gas Shift behavior:

The catalytic activity of the studied gold catalysts is presented in **Figure 5A**. It is worth to mention that the parent supports of the presented gold catalysts resulted to be hardly active in the WGS thus underlining the importance of the metallic phase for achieving good performances. As expected the CO conversion increases on raising temperature but the shape of the conversion *vs.* temperature curve is affected by the catalyst nature reflecting the influence of the catalysts composition on their kinetic parameters.

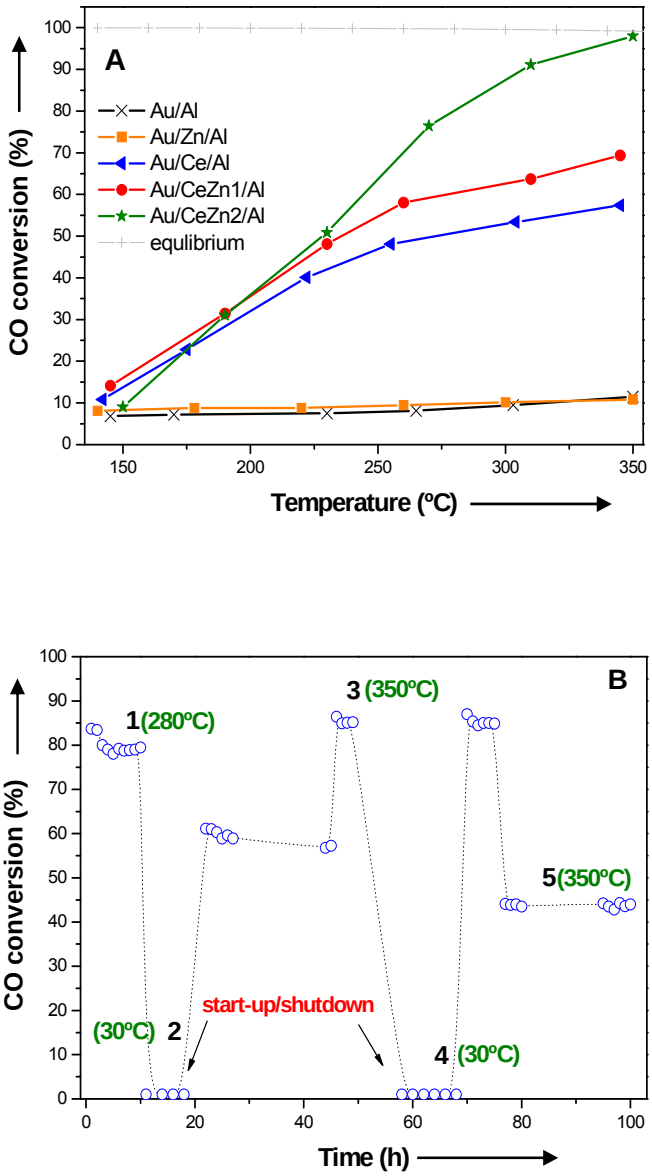

Figure 5: WGS catalytic study: A) activity test B) long-term stability of Au/CeZn2/Al under different conditions: 1) 4.5% CO + 30% H_2O in N_2 at 280ºC; 2) start-up/shutdown 3) 4.5% CO + 30% H_2O in N_2 at 350ºC; 4) start-up/shutdown 5) 9% CO + 11% CO_2 + 50% H_2 + 30% H_2O at 350ºC.

As can be deduced from the plot, the CO conversion followed the next activity order:

Au/CeZn2/Al › Au/CeZn1/Al › Au/Ce/Al › ›Au/Zn/Al › Au /Al

The result clearly manifests that ceria presence in the catalyst formulation is totally necessary for the activity in WGS since the materials without ceria are hardly active in the reaction. The later agrees with the proposal of Rodriguez´s group for a gold catalyst in the WGS [23]. As gold is not capable of developing any water splitting, the activation of water in a gold based catalyst obligatorily requires the presence of an "active" support with structural defects where water can be activated, as for example cerium oxide. Furthermore, the presence of ZnO enhanced the catalytic performance of the Au/Ce/Al catalyst. The CO conversion increased with the amount of ZnO, revealing the positive effect of this promoter. Indeed we have recently reported the beneficial effect of the ZnO addition to a CeO_2-Al_2O_3 commercial support for CO oxidation reactions [24]. In this work, it was demonstrated that the Zn-doped solids show a superior catalytic activity compared to the bare CeO_2-Al_2O_3 due to the intimate contact of the ZnO and CeO_2 phases, at which interface an exchange of the lattice oxygen occurs. The later correlates with the result obtained from the OSC, OSCC and UV-Vis data in terms of modification of the ceria electronic properties and oxygen mobility due to the addition of ZnO to CeO_2. The superior availability of the oxygen in the Zn-doped samples potentiates the redox mechanisms through which the WGS reaction most likely proceed in these samples. The most active sample reached 98.5% of CO conversion (which is the equilibrium conversion) at 350ºC, temperature for which the NL is the maximum and involves the participation of oxygen from the eighth ceria bulk layer, which corresponds to the maximum amount of available oxygen. The enhanced redox properties are associated to electronics perturbations due to the strong metal-support contact. As proposed by Campbell this kind of metal particles-support interactions could explain the excellent catalytic activity [25].

In order to compare with previous result from the literature, the specific reaction rates expressed as $mol_{COconverted}.g_{Au}^{-1}.\ s^{-1}$at 250ºC and the measured turnover frequency (TOF) in s^{-1} have been calculated and they are presented in **Table 5.** TOF is calculated as in ref. [26] with the following equation:

$$TOF = \frac{r_{CO}\,.\,M_{Au}}{D_{Au}}\ [s^{-1}]$$

Where r_{CO} is the reaction rate in $mol_{COconverted}.mol_{Au}^{-1}\ s^{-1}$, M_{Au} is the atomic weight of gold (196.95 g mol^{-1}) and D_{Au} is gold dispersion. In all cases, gold dispersion has been estimated to be 32% on the basis of the hemispherical ball model proposed by Polisset [27] and assuming an average gold particle size of 4 nm, as discussed above.

From **Table 5** it can be understood that the gold-supported γ-alumina catalyst demonstrates poor activity in the WGS reaction. The Zn-Ce mixed systems presented the highest reaction rates and TOF values. The most efficient catalyst (Au/CeZn2/Al) reached reaction rates of 7.18 $mol_{COconverted}.g_{Au}^{-1}.\ s^{-1}$. Moreover this material, exhibited superior activity, in terms of reaction rates and TOF, compare to similar Au/Ce (4.2 $mol_{COconverted}.g_{Au}^{-1}.\ s^{-1}$) and Au/Ce/Al (1.8 $mol_{COconverted}.g_{Au}^{-1}.\ s^{-1}$) catalysts well referenced in the literature [10a, 28]. The obtained catalytic data correlate with the promotion of ceria redox properties by the addition of small amounts of ZnO to CeO_2. This

could indicate that the redox mechanism is the one that control the WGS process. Thus, the higher OSC of the Au/CeZn2/Al sample results in a higher catalytic performances due to its higher oxygen mobility.

For a possible industrial application not only the activity but also the stability of the catalyst is a matter to consider. A long-term stability test under different reaction conditions and combining start-up/shut-down cycles of the most active sample (Au/CeZn2/Al) is presented in **Figure 5B**. At 280ºC the system losses some activity (5 % of CO conversion) in the first hours of reaction. However after 7 hours the system reaches the steady state maintaining high CO conversion (point 1 in the graph). The first start-up/shut-down operation was applied in this moment (point 2). The system was cooled under reaction flow till room temperature and maintained at this temperature (*ca*. 30ºC) during some hours, which means that liquid water will cover the catalytic bed.

Table 5. WGSR reaction rates (r) in $mol_{COconverted}.g_{Au}^{-1}$ $s^{-1}*10^5$ and TOF_s in s^{-1} $*10^2$ measured at 250ºC

Catalysts	r	TOF
Au/Al	1,53	0.92
Au/Ce/Al	6.12	3.69
Au/Zn/Al	3.06	1.80
Au/CeZn1/Al	6.52	3.93
Au/CeZn2/Al	7.18	4.32

This methodology of start/stop cycles has been proposed by Farrauto and coworkers and it is considered as one of the most severe deactivation processes that can be applied on a WGS catalyst and try to imitate a possible start/stop situation in a real application [29]. Complete recuperation of the CO conversion was not obtained when the temperature was raised again up to 280ºC. Indeed, after this treatment the CO conversion was 60%, which represents a loss of activity of about 20%. The catalyst deactivation is likely due to the formation of stable carbonate species in the catalysts surface that blocks the active sites for water splitting thus reducing the activity in the WGS. In fact, the deactivation due to the formation of these species has been previously demonstrated using TPD/TPO techniques for a very similar gold based system [30]. The study of the possible blocking species is not the subject of this paper. However, in an attempt to improve the CO conversion, the temperature was raised up to 350ºC (point 3 in the figure). After this thermal treatment the activity remarkable increased. The later means that the carbonates blocking species can be eliminated and the activity recovered by increasing the temperature as reported in ref. [30]. After several hours conserving high conversions at 350ºC, a second start/stop cycle was carried out (point 4 in the figure). This time, the system completely recovered its activity after the shutdown. This may be due to the instability of the blocking species at such a high temperature. In any case, this result is very promising since the Au/CeZn2/Al catalysts is able to keep high values of CO conversion without any apparent deactivation and, more importantly, it is able to tolerate the start-up/shut-down cycles. Finally a realistic reformate gas mixture was considered to test the resistance of the catalysts in a more aggressive atmosphere (point 5). As expected, the CO conversion drops under these conditions. Several reasons may account for this fact: i) the obvious shift of the equilibrium according to LeChatelier principle ii) the over-reduction of ceria in a more reductive environment iii) the suppression of the redox mechanism. The ability of water to re-oxide the support (which is a key step on the redox mechanism) is limited in such a reductive gas mixture. In addition, Goguet and co-workers reported that the prolonged exposure to elevated amounts of CO_2 in the presence of water influences the structure of the gold nanoparticles and promotes the dewetting of the nanoparticles from the support thus decreasing the catalytic activity [31]. Despite the observed deactivation, it should be underlined that the system exhibited a very good stability under the realistic post-reforming stream. Under a model WGS mixture (4.5% CO and 30 % H_2O) with Au/CeZn2/Al catalyst, the equilibrium conversion can be achieved and 1% of CO will be present in the PrOx inlet.

Conclusions

In the present work a series of $Au/CeO_2/Al_2O_3$ catalysts doped with ZnO is proposed for CO free hydrogen production. XRD and TEM data confirmed that all the solids are composed by small gold nanoparticles well dispersed on the support. The presence of ZnO was evidenced by UV-vis spectroscopy. The ZnO-doped samples present high activity the for WGS process. The high activity of this samples compared to the un-promoted gold-ceria-alumina is mainly related to the superior oxygen storage capacity and enhanced reducibility obtained when ZnO is added to the catalyst formulation.

The surface/ bulk ceria oxygen ratio has been demonstrated and this contribution is higher when ZnO is added to CeO_2 leading to a high performance in the studied reactions. Very good stability was obtained for the Au/CeZn2/Al sample. In addition, as a very promising result, this sample successfully tolerate the start-up/shut-down cycles at 350ºC which is of crucial relevance for a real application. Considering findings mentioned above in combination with the economic feasibility of this novel catalytic system, it can be concluded that the Au/CeZn/Al catalysts constitute a promising alternative for the pure hydrogen production.

Experimental

Catalyst preparation

Support preparation

The supports were synthesized by a conventional co-precipitation method. The necessary amounts of metal precursor zinc nitrate (99.9% Aldrich) or cerium nitrate (99.5%, Aldrich) were impregnated on γ-alumina powder (Sasol). The impregnation was carried out in 50 mL of ethanol and the solvent was evaporated till obtaining of a dry solid in rotary vapour at reduced pressure and temperature of 50ºC. The obtained solid was treated with NH_3 solution (10 $mol.L^{-1}$) during 30 min in order to assure the full conversion of the nitrates to hydroxides. Finally it was filtered, dried at 100ºC and calcined at 500ºC for 4 hours.

Cerium oxide amount was fixed at 15 wt.% and, for the ZnO, 1 and 2 wt.% was intended. For the mixed oxides also 15 wt. % of CeO_2-ZnO mixed oxide was targeted. In the adopted nomenclature the oxygen is omitted for simplification and the

dopant (ZnO) contents are expressed as the theoretical loading in the catalysts. For example, the CeZn2/Al solid contains 15 wt.% Ce-Zn mixed oxide in which the ZnO loading is 2 wt.%., deposited on Al_2O_3.

Gold deposition

The gold was deposited by the direct anionic exchange method (DAE), assisted by NH_3 as described elsewhere [32]. $2x10^{-4}$ M Aqueous solutions of the gold precursor $HAuCl_4$ (49.81 % Johnson Matthey) and support sieved in between 100-200 μm were used in order to obtain a final Au loading of 2 wt.%. The solution was heated to 70ºC and aged 20 min. After that, it was cooled down to 40ºC and 50 mL of NH_3 (30 % Aldrich) ware added. The slurry was then filtered, washed with water, dried in an oven at 100°C overnight and calcined in air at 350°C for 4 h.

Similar to the supports, in the adopted nomenclature the real gold loadings are omitted for simplification and the ZnO contents are expressed as the theoretical wt.% loading in the catalysts. For example, the Au/CeZn2/Al solid contains 2 wt.% of Au over 15 wt.% of Ce-Zn mixed oxide on Al_2O_3 support in which the ZnO loading is 2 wt.% approximately.

Characterization

The chemical composition of the samples was determined by X-Ray microfluorescence spectrometry (XRMF) in an EDAX Eagle III spectrophotometer with a rhodium source of radiation working at 40 KV.

The textural properties were studied by N_2 adsorption-desorption measurements at liquid nitrogen temperature. The experiments were carried out on a Micromeritics ASAP 2010 instrument. Before analysis, the samples were degassed for 2 h at 150º C in vacuum. The Barrett-Joyner-Halenda (BJH) method was used for determining the pore size distributions, and in every case the desorption isotherm was used.

X-ray diffraction (XRD) analysis was performed on an X'Pert Pro PANalytical. Diffraction patterns were recorded with Cu Kα radiation (40 mA, 45 kV) over a 2θ-range of 10 to 80º and a position-sensitive detector using a step size of 0.05º and a step time of 240 s.

High-Resolution Transmission Electron Microscopy (HRTEM) and High-Angle Annular Dark Field-Scanning Transmission Electron Microscopy (HAADF-STEM) images were recorded on a JEOL2010F instrument. The spatial resolution at Scherzer defocus conditions in HRTEM mode is 0.19 nm, while the HAADF-STEM studies were performed using an electron probe of 0.5 nm of diameter and a diffraction camera length of 10 cm. It should be pointed that the chemical composition of the sample was studied in STEM mode using an Energy-dispersive X-ray spectrometer (Oxford Instrument, Inca Energy-200).

The UV-Vis spectra were recorded on a Varian spectrometer model Cary 100, equipped with integrating sphere and using $BaSO_4$ as reference. All the spectra were collected in a diffuse reflectance mode and transformed to a magnitude proportional to the extinction coefficient through the Kubelka-Munk function F(α).

For the Oxygen Storage Complete Capacity (OSCC) 100 mg of catalyst was loaded into a U-shaped quartz reactor and the temperature was raised in a He flow (50 mL/min) until 350 ºC. Then, ten O_2 pulses of 1 mL were injected every 2 min. After that, the sample is submitted to ten CO pulses of 1 mL each (every 2 min). The sample is then degassed during 10 min in a He flow, subjected to a new series of oxidizing pulses (ten O_2 pulses) and then exposed to five alternating pulses ($CO–O_2–CO–O_2–CO$). The Oxygen Storage Capacity (OSC) is determined by the amount of CO_2 formed after the first CO pulse of the alternated ones. This method is based on the one presented by Duprez et al. [33]. The gas composition at the exit of the reactor was analyzed by a mass spectrometer PFEIFFER Vacuum PrismaPlus controlled by the program Quadera®.

Catalytic activity

Water-gas shift reaction was performed in a flow reactor at atmospheric pressure in the temperature range of 140-350 ºC. The following conditions were applied: catalyst bed volume 0.5 cm^3, space velocity 4000 h^{-1}, partial pressure of water vapour 31.1 kPa and the reactant gas mixture containing 4.494 vol.% CO in argon. The CO and CO_2 content was analyzed on ''URAS-3G'' and ''URAS- 2T'' (Hartmann &Braun AG) gas analyzers and the catalytic activity was expressed in % of CO conversion.

Acknowledgements

T. R.Reina acknowledges CSIC for his JAE-Predoc fellowship co-financed with the European social program and S. Ivanova MEC for her Ramon y Cajal contract. The Spanish Ministerio de Ciencia e Innovación under contract (ENE2012-374301-C03-01) and Junta de Andalucía under the contract TEP-8196 provide financial support for this work, both programs are co-funded by the European Union FEDER. The authors are also grateful for the financial support offered by the CSIC-BAS project 2009B60024. Dr. Alejandro Pérez Flórez is also acknowledged for his contribution. The authors thank Sasol for providing the alumina.

Keywords: Gold catalysts, CO removal, WGS, H_2 purification

References

[1] L. M. Gandía, G. Arzamendi and P. M. Diéguez in *Chapter 1 - Renewable Hydrogen Energy: An Overview*, *Vol.* Eds.: L. M. Gandía, G. Arzamendi and P. M. Diéguez), Elsevier, Amsterdam, **2013**, pp. 1-17.

[2] S. Ivanova, O. H. Laguna, M. Á. Centeno, A. Eleta, M. Montes and J. A. Odriozola in *Chapter 10 - Microprocess Technology for Hydrogen Purification*, *Vol.* Eds.: L. M. Gandía, G. Arzamendi and P. M. Diéguez), Elsevier, Amsterdam, **2013**, pp. 225-243.

[3] G. Arzamendi, P. M. Diéguez, M. Montes, M. A. Centeno, J. A. Odriozola and L. M. Gandía, *Catalysis Today* **2009**, *143*, 25-31.

[4] a) Q. Fu, S. Kudriavtseva, H. Saltsburg and M. Flytzani-Stephanopoulos, *Chemical Engineering Journal* **2003**, *93*, 41-53; b) D. Andreeva, V. Idakiev, T. Tabakova, L. Ilieva, P. Falaras, A. Bourlinos and A. Travlos, *Catalysis Today* **2002**,

72, 51-57; c) H. Sakurai, T. Akita, S. Tsubota, M. Kiuchi and M. Haruta, *Applied Catalysis A: General* **2005**, *291*, 179-187; d) D. Andreeva, V. Idakiev, T. Tabakova and A. Andreev, *Journal of Catalysis* **1996**, *158*, 354-355; e) O. H. Laguna, F. Romero Sarria, M. A. Centeno and J. A. Odriozola, *Journal of Catalysis* **2010**, *276*, 360-370.

[5] T. Tabakova, L. Ilieva, I. Ivanov, R. Zanella, J. W. Sobczak, W. Lisowski, Z. Kaszkur and D. Andreeva, *Applied Catalysis B: Environmental* **2013**, *136–137*, 70-80.

[6] R.Burch *Physical Chemistry Chemical Physics* 8 (2006) 5483-5500.

[7] a) Q. Fu, H. Saltsburg and M. Flytzani-Stephanopoulos, *Science* **2003**, *301*, 935-938; b) Q. Fu, W. Deng, H. Saltsburg and M. Flytzani-Stephanopoulos, *Applied Catalysis B: Environmental* **2005**, *56*, 57-68; c) T. Tabakova, G. Avgouropoulos, J. Papavasiliou, M. Manzoli, F. Boccuzzi, K. Tenchev, F. Vindigni and T. Ioannides, *Applied Catalysis B: Environmental* **2011**, *101*, 256-265.

[8] A. Trovarelli, *Catalysis Reviews - Science and Engineering* **1996**, *38*, 439-520.

[9] A. Penkova, O. H. Laguna, M. A. Centeno and J. A. Odriozola, *Journal of Physical Chemistry C* **2012**, *116*, 5747-5756.

[10] a) T. Tabakova, M. Manzoli, D. Paneva, F. Boccuzzi, V. Idakiev and I. Mitov, *Applied Catalysis B: Environmental* **2011**, *101*, 266-274; b) G. Xiao, S. Li, H. Li and L. Chen, *Microporous and Mesoporous Materials* **2009**, *120*, 426-431; c) G. Avgouropoulos and T. Ioannides, *Journal of Molecular Catalysis A: Chemical* **2008**, *296*, 47-53; d) T. Tabakova, V. Idakiev, D. Andreeva and I. Mitov, *Applied Catalysis A: General* **2000**, *202*, 91-97.

[11] O. H. Laguna, M. A. Centeno, F. Romero-Sarria and J. A. Odriozola, *Catalysis Today* **2011**, *172*, 118-123.

[12] S. Ivanova, V. Pitchon and C. Petit, *Journal of Molecular Catalysis A: Chemical* **2007**, *272*, 306.

[13] Z. Kónya, V. F. Puntes, I. Kiricsi, J. Zhu, J. W. Ager Iii, M. K. Ko, H. Frei, P. Alivisatos and G. A. Somorjai, *Chemistry of Materials* **2003**, *15*, 1242-1248.

[14] M. Á. Centeno, C. Portales, I. Carrizosa and J. A. Odriozola, *Catalysis Letters* **2005**, *102*, 289-297.

[15] J. Geng, G.-H. Song, X.-D. Jia, F.-F. Cheng and J.-J. Zhu, *The Journal of Physical Chemistry C* **2012**, *116*, 4517-4525.

[16] A. A. A. Ahmed, Z. A. Talib, M. Z. B. Hussein and A. Zakaria, *Journal of Alloys and Compounds* **2012**, *539*, 154-160.

[17] S. Talam, S. R. Karumuri and N. Gunnam, *ISRN Nanotechnology* **2012**, *2012*, 6.

[18] M. A. Centeno, M. Paulis, M. Montes and J. A. Odriozola, *Applied Catalysis A: General* **2002**, *234*, 65-78.

[19] Y. Kim and S. Kang, *The Journal of Physical Chemistry B* **2010**, *114*, 7874-7878.

[20] N.Acerbi,S. Golunski, S.C.Tsang, H.Daly, C.Hardacre, R.Smith and P.Collier, *The Journal of Physical Chemistry C* **2012**, *116*, 13569-13583.

[21] S. Bedrane, C. Descorme and D. Duprez, *Catalysis Today* **2002**, *75*, 401-405.

[22] Y. Madier, C. Descorme, A. M. Le Govic and D. Duprez, *The Journal of Physical Chemistry B* **1999**, *103*, 10999-11006.

[23] a) J. A. Rodriguez, *Catalysis Today* **2011**, *160*, 3-10; b) J. B. Park, J. Graciani, J. Evans, D. Stacchiola, S. D. Senanayake, L. Barrio, P. Liu, J. F. Sanz, J. Hrbek and J. A. Rodriguez, *Journal of the American Chemical Society* **2009**, *132*, 356-363.

[24] T. R. Reina, S. Ivanova, M. I. Domínguez, M. A. Centeno and J. A. Odriozola, *Applied Catalysis A: General* **2012**, *419–420*, 58-66.

[25] C.T. Campbell, *Nature Chemistry* **2012**, *4,* 597-598.

[26] Y.-F. Han, Z. Zhong, K. Ramesh, F. Chen and L. Chen, *The Journal of Physical Chemistry C* **2007**, *111*, 3163-3170.

[27] M. Polisset, Ph. D. Thesis University of Paris VI, **1990.**

[28] D. Andreeva, I. Ivanov, L. Ilieva and M. V. Abrashev, *Applied Catalysis A: General* **2006**, *302*, 127-132.

[29] a) W. Ruettinger, X. Liu and R. J. Farrauto, *Applied Catalysis B: Environmental* **2006**, *65*, 135-141; b) R. Farrauto, Y. Liu, W. Ruettinger, O. Ilinich, L. Shore and T. Giroux, *Catalysis Reviews - Science and Engineering* **2007**, *49*, 141-196.

[30] T. R. Reina, S. Ivanova, V. Idakiev, J. J. Delgado, I. Ivanov, T. Tabakova, M. A. Centeno and J. A. Odriozola, *Catalysis Science and Technology* **2013**, *3*, 779-787.

[31] H.Daly, A.Goguet, F.C. Meunier, R.Pilasombat, D. Thompsett, *Journal of Catalysis* 273 (2010) 257-265.

[32] S. Ivanova, C. Petit and V. Pitchon, *Applied Catalysis A: General* **2004**, *267*, 191-201.

[33] a) S. Kacimi, J. Barbier Jr, R. Taha and D. Duprez, *Catalysis Letters* **1993**, *22*, 343-350; b) S. Royer and D. Duprez, *ChemCatChem* **2011**, *3*, 24-65.

Received: ((will be filled in by the editorial staff))
Published online: ((will be filled in by the editorial staff))

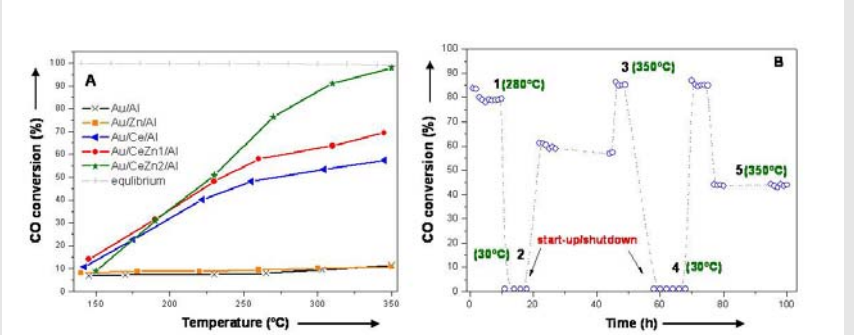

A series of gold catalysts supported on ZnO-promoted CeO_2-Al_2O_3 is presented as interesting systems for the purification of H_2 streams via WGS.
The addition of ZnO remarkably promotes the activity of a $Au/CeO_2/Al_2O_3$ catalyst.
This increase in activity is mainly associated to the enhanced OSC exhibited for the Zn-containing solids. The prepared catalysts tolerate start/stop cycles under operation, which is a very important skill for a possible industrial application.

*Svetlana Ivanova,Juan Jose Delgado, Ivan Ivanov, Vasko Idakiev ,Tatyana Tabakova, Miguel Angel Centeno, José Antonio Odriozola and Tomás Ramírez Reina**

Page No. 1 – Page No. 8

Viability of Au/CeO_2-ZnO/Al_2O_3 catalysts for pure hydrogen production via WGS